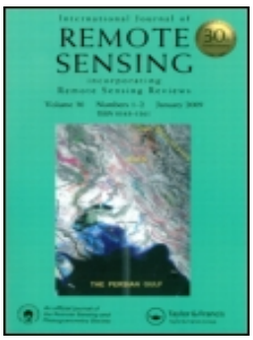

International Journal of Remote Sensing

ISSN: 0143-1161 (Print) 1366-5901 (Online) Journal homepage: http://www.tandfonline.com/loi/tres20

On the application of the MODTRAN4 atmospheric radiative transfer code to optical remote sensing

Luis Guanter , Rudolf Richter & Hermann Kaufmann

To cite this article: Luis Guanter , Rudolf Richter & Hermann Kaufmann (2009) On the application of the MODTRAN4 atmospheric radiative transfer code to optical remote sensing, International Journal of Remote Sensing, 30:6, 1407-1424, DOI: 10.1080/01431160802438555

To link to this article: http://dx.doi.org/10.1080/01431160802438555

Published online: 22 Apr 2009.

International Journal of Remote Sensing
Vol. 30, No. 6, 20 March 2009, 1407–1424

Taylor & Francis
Taylor & Francis Group

On the application of the MODTRAN4 atmospheric radiative transfer code to optical remote sensing

LUIS GUANTER*†, RUDOLF RICHTER‡ and HERMANN KAUFMANN†
†GFZ – GeoForschungsZentrum Potsdam, Remote Sensing Section, Telegrafenberg, D-14473, Potsdam, Germany
‡DLR – German Aerospace Center, Remote Sensing Data Center, D-82234, Wessling, Germany

(*Received 15 August 2008; in final form 8 December 2008*)

The quantification of atmospheric effects on the solar radiation measured by a spaceborne or airborne optical sensor is required for some key tasks in remote sensing, such as atmospheric correction, simulation of realistic scenarios or retrieval of atmospheric parameters. The MODTRAN4 code is an example of state-of-the-art atmospheric radiative transfer code, as it provides very accurate calculations by means of a rigorous mathematical formulation and a very fine spectral resolution. However, the application of MODTRAN4 to remote sensing is not straightforward for the average user for a number of reasons: the provided output parameters do not exactly correspond to those necessary for the construction of the at-sensor signal by combination with the surface reflectance, an advanced knowledge of radiative transfer theory and atmospheric physics is needed for the understanding of the input parameters and all their possible combinations, and the computation time may be too high for many practical applications. This work is intended to give explicit solutions to those problems. MODTRAN4 has been modified so that the proper atmospheric parameters are calculated and delivered as output. In addition, the most important execution options are investigated, and the compromise between accuracy and computation time is analysed. The performance of the proposed methodology is demonstrated by generating a look-up table (LUT) enabling fast but accurate radiative transfer calculations for the atmospheric correction of data acquired by the Compact High Resolution Imaging Spectrometer (CHRIS) on board the Project for On-Board Autonomy (PROBA).

1. Introduction

The strong interaction between the atmospheric components and the solar radiation travelling across the atmosphere makes the modelling and quantification of atmospheric radiative transfer a major issue in the analysis of optical remote sensing data. The simulation of the electromagnetic solar radiation which is measured by a sensor on board a satellite or an airborne platform is not only the starting point for most of atmospheric correction methods (those working on the removal of the distortion caused by the atmospheric components on the reflected electromagnetic signal), but it is also necessary for other tasks, such as the generation of synthetic data for mission simulators or the estimation of atmospheric parameters from inversion techniques.

*Corresponding author. Email: luisguan@gfz-potsdam.de

International Journal of Remote Sensing
ISSN 0143-1161 print/ISSN 1366-5901 online
http://www.tandf.co.uk/journals
DOI: 10.1080/01431160802438555

The proper evaluation of the interaction of radiation with surface and atmosphere is normally achieved by the use of atmospheric radiative transfer codes (RTCs). These provide numerical solutions of the radiative transfer equation for a given set of input parameters describing the physical scenario and the computational set-up. The MODTRAN4 code (Berk *et al.* 1998, 2003) is one of the most widely used RTCs in accurate simulations of atmospheric radiative transfer. It is a general-purpose atmospheric simulator, which reproduces the radiances at the sensor level with a spectral resolution up to $1\,cm^{-1}$. The rigorous coupling of absorption and scattering events in the physical formulation enables accurate calculations even inside strong atmospheric absorption features. Examples of applications using MODTRAN4 are mostly in the field of atmospheric correction (Staenz and Williams 1997; Adler-Golden *et al.* 1999; Richter and Schlaepfer 2002; Miller 2002; Miesch *et al.* 2005; Guanter *et al.* 2007), but there are also codes for sensor simulation (Börner *et al.* 2001), generation of realistic scenarios (Verhoef and Bach 2003, 2007), or assessment of instrument's calibration (Green 1998; Green *et al.* 2003; Guanter *et al.* 2006) using MODTRAN4 as well. The topic of the simulation of atmospheric radiative transfer is also a key tool in the field of climate research (Henzing *et al.* 2004; Ogunjobi and Kim 2007; Kondratyev and Varotsos 1995).

Some major problems appear when MODTRAN4 is to be applied to remote sensing. First of all, it is a 'forward' RTC, which means that it is intended to generate top-of-atmosphere (TOA) radiances (or, equivalently, at-sensor radiances if the sensor is inside the atmosphere) from given atmospheric and surface conditions. Applying it in 'backward' mode, as it is the case of the retrieval of surface reflectance from TOA radiances, is not straightforward, because the necessary atmospheric functions are not included in the standard MODTRAN4 output, but have to be computed separately. In particular, the atmospheric path radiance, the transmittance for direct and diffuse radiation, the direct and diffuse fluxes and the spherical albedo are sufficient for the parametrization of the atmospheric radiative transfer and the inversion of TOA radiances. Those parameters must be decoupled from the surface reflectance so that they depend only on the atmospheric state, the solar and sensor viewing geometries and the surface elevation. Furthermore, the separation between direct and diffuse at-surface fluxes, as well as between the transmittance for direct and diffuse radiation, enables the consideration of directional effects (Vermote *et al.* 1997a; Verhoef and Bach 2003), topographic effects (Richter 1998; Hay 1979) or adjacency effects (Dave 1980; Mekler and Kaufman 1982; Kaufman 1984; Vermote *et al.* 1997a) in the whole radiative transfer scheme.

On the other hand, the mathematical coupling between scattering and absorption in every atmospheric path causes MODTRAN4 to have prohibitive computation times when a large number of runs is necessary, as it is the case of iterative inversion routines or the compilation of look-up tables (LUTs). Moreover, a vast knowledge about atmospheric radiative transfer is needed in order to fully understand most of MODTRAN4 execution options, the input and output files or the best trade-off between accuracy and computation time for a given application. For example, the improvement in accuracy associated with the use of the discrete-ordinate radiative-transfer (DISORT) method (Stamnes *et al.* 1988) for multiple scattering calculations, or the correlated-k treatment for the computation of radiation absorption, are counterbalanced by important increases in computation time, which may not be justified by the requirements imposed by a given application. For these reasons, other more efficient but less accurate RTCs are often preferred for remote sensing

applications, such as the Second Simulation of the Satellite Signal in the Solar Spectrum (6S) code (Vermote *et al.* 1997b).

The aim of this paper is to provide practical solutions to the previous issues. The derivation of the suitable atmospheric optical parameters for the construction of the TOA signal is achieved by means of some algebra performed over the standard MODTRAN4 outputs. Two runs with different background reflectance are needed for this purpose. The resulting code driving the two loops and managing the results has been called ATLUT. It intends to adapt MODTRAN4 itself to the flexibility and efficiency requirements imposed by remote sensing. It can be used in forward or backward atmospheric simulations, or in an iterative scheme to generate LUTs which would provide the atmospheric parameters by interpolation. The modifications of the original code are done at the source code level, generating a faster executable file providing directly the atmospheric functions. In addition, some MODTRAN4 subroutines have been modified so that the retrieval of the spectral radiances and fluxes needed for the calculation of the atmospheric parameters are not written to an external file, but they are internally passed to a driver subroutine in charge of the data management.

The mathematical background supporting the ATLUT code, theoretical considerations about the inclusion of directional, topographic and adjacency effects on the TOA radiance formulation, as well as some guidelines for the compilation of a general-purpose LUT, are discussed in §2. Section 3 presents results about two different topics. Firstly, options for radiative transfer calculations in MODTRAN4/ATLUT have been analysed. The study is mainly focused on finding the best compromise between computation time and calculation accuracy for multiple scattering (use of DISORT) and absorption calculations (concerning band model and correlated-k treatment). Secondly, the performance of the proposed methodology is demonstrated by the application of ATLUT to the compilation of a LUT devoted to the atmospheric correction of hyperspectral data. The Compact High Resolution Imaging Spectrometer (CHRIS) on board the Project for On-Board Autonomy (PROBA) system (Barnsley *et al.* 2004) has been selected as a case study because of its particular angular and spectral characteristics. Finally, a summary of the main findings is provided in §4.

2. Methodology

2.1 *Mathematical background for the decoupling of atmospheric optical parameters*

The radiation reflected by the atmosphere into the sensor's line-of-sight, known as atmospheric path radiance, and the total radiance at the sensor level for a surface with reflectance ρ ($L_p(\rho)$ and $L_{TOA}(\rho)$, respectively) are given in MODTRAN4 by (Richter 1990):

$$L_p(\rho) = L_p(0) + t_{dif}^{\uparrow} E_g(\rho)\rho \Big/ \pi \tag{1}$$

and

$$L_{TOA}(\rho) = L_p(\rho) + t_{dir}^{\uparrow} E_g(\rho)\rho \Big/ \pi, \tag{2}$$

where $t_{dif}^{\uparrow}$ and $t_{dir}^{\uparrow}$ are the spectral transmittances for diffuse and direct radiation, respectively, travelling upwards from the surface to the sensor, and E_g is the global flux reaching the surface. For a horizontal surface this can be written as,

$$E_g(\rho) = E_{dir}\mu_s + E_{dif}(\rho), \tag{3}$$

E_{dir}, E_{dif} being the direct and diffuse fluxes at ground level, and μ_s the cosine of the solar zenith angle. The multiple scattering between the atmosphere and the surface is computed in equations (1) and (2) by means of the diffuse flux $E_{dif}(\rho)$ component, which is coupled to the surface reflectance. Since the aim of the ATLUT program is to obtain atmospheric parameters independent of the surface reflectance, equation (2) must be rewritten to eliminate the dependence of the atmospheric parameters on ρ. It can be expressed as

$$L_{TOA}(\rho) = L_p(0) + \frac{T^{\uparrow}E_g(0)\rho/\pi}{1-\rho S}, \tag{4}$$

where S is the atmospheric spherical albedo accounting for multiple scattering between atmosphere and surface, and $T^{\uparrow}$ is the total transmittance, $T^{\uparrow} = t^{\uparrow}_{dir} + t^{\uparrow}_{dif}$. It can be stated that ρ can be analytically inverted from L_{TOA} in equation (4), as all the variables are independent of ρ. Thus, $L_p(0)$, $t^{\uparrow}_{dir}$, $t^{\uparrow}_{dif}$, $E_g(0)$, and S must be calculated as the initial step in the atmospheric correction procedure. It must noted that a Lambertian surface is assumed (Nicodemus *et al.* 1977), and that ρ represents then the surface spectral albedo.

The term $t^{\uparrow}_{dir}$ is directly given by MODTRAN4 as output. Concerning the fluxes, the explicit separation of E_{dir}, $E_{dif}(0)$ is highly convenient if directional, topographic or adjacency effects are to be taken into account in the atmospheric modelling. The fluxes can be retrieved either from the radiance calculations or from MODTRAN4's flux file. Nevertheless, since the fluxes directly calculated by the spcflx.f subroutine may be inaccurate in spectral regions with strong gaseous absorptions, they are retrieved from the radiances in routine trans.f, using

$$E_{dir} = \frac{\pi L_{r,\,dir}}{\mu_s t^{\uparrow}_{dir}\rho} \tag{5}$$

$$E_{dif}(\rho) = \frac{\pi L_{r,\,TOA}}{t^{\uparrow}_{dir}\rho} - \mu_s E_{dir} \tag{6}$$

where $L_{r,dir}$ and $L_{r,TOA}$ are the direct and total reflected radiances, respectively, reaching the sensor after being reflected by the target surface.

Concerning $L_p(0)$, $t^{\uparrow}_{dif}$ and S, it can be shown from equations (1)–(4) that they can be computed from two MODTRAN4 runs, with two different values of the surface reflectance, ρ_1 and ρ_2. With a little algebra:

$$L_p(0) = \frac{L_p(\rho_2)\rho_1 E_g(\rho_1) - L_p(\rho_1)\rho_2 E_g(\rho_2)}{\rho_1 E_g(\rho_1) - \rho_2 E_g(\rho_2)}, \tag{7}$$

$$t^{\uparrow}_{dif} = \frac{\pi\left[L_p(\rho_1) - L_p(0)\right]}{\rho_1 E_g(\rho_1)} \tag{8}$$

and

$$S = \frac{E_g(\rho_2) - E_g(\rho_1)}{\rho_2 E_g(\rho_2) - \rho_1 E_g(\rho_1)}. \tag{9}$$

Values of $\rho_1=0.5$ and $\rho_2=0.15$ have been selected for the reflectance background representing high and medium reflectances of natural targets. The use of $\rho=0$ is avoided because this could lead to some inconsistencies with some of the MODTRAN4 options. For example, the MODTRAN4 scaled-DISORT option is the best one for those applications in which the maximum accuracy inside absorption regions is not a requisite. The scaling is not performed by MODTRAN4 over E_{dif} for a black surface ($\rho=0$), leading to significant miscalculations of the spherical albedo that cause substantial errors in the TOA radiances expressed in equation (4). Moreover, if $\rho=0$ equations (5) and (6) cannot be applied for the calculation of the fluxes from the TOA radiances. These reasons justify that $0<\rho_{1,2}<1$. Neither from the mathematical point of view nor from the physical one is there any constraint for the selection of $\rho_{1,2}$.

2.2 *Considerations on directional effects*

The coupling between atmospheric radiative transfer and surface directional effects is necessary for the most accurate simulations of those targets deviating from the Lambertian behaviour. Equation (4) must then be extended so that directional effects are considered in the target reflectance. If a suitable model for the bidirectional reflectance distribution function (BRDF) is available, the extension of the Lambertian assumption is possible using the separation of the radiative transfer parameters provided by ATLUT.

Following Vermote *et al.* (1997b) and Verhoef and Bach (2003, 2007), the contribution of the target to the upward TOA radiances is decomposed as the sum of four terms: (a) the photons directly transmitted from the Sun to the target and directly reflected back to the sensor, (b) the photons scattered by the atmosphere then reflected by the target and directly transmitted to the sensor, (c) the photons directly transmitted to the target but scattered by the atmosphere on their way to the sensor, and finally (d) the photons having at least two interactions with the atmosphere and one with the target. Adapting the mathematical formalisms in Vermote *et al.* (1997b) and Verhoef and Bach (2007), πL_{TOA} can be written as

$$\pi L_{\mathrm{TOA}}=\pi L_{\mathrm{p}}(0)+t_{\mathrm{dir}}^{\uparrow}\left[\rho_s E_{\mathrm{dir}}+\bar{\rho}E_{\mathrm{dif}}^{*}\right]+t_{\mathrm{dif}}^{\uparrow}\left[\bar{\rho}'E_{\mathrm{dir}}+\bar{\bar{\rho}}E_{\mathrm{dif}}^{*}\right]+T^{\uparrow}E_{\mathrm{g}}^{*}S\bar{\bar{\rho}}^{2} \tag{10}$$

where

$$E_{\mathrm{dif}}^{*}=\frac{E_{\mathrm{dif}}(0)}{1-S\bar{\bar{\rho}}} \tag{11}$$

and

$$E_{\mathrm{g}}^{*}=\frac{E_{\mathrm{g}}(0)}{1-S\bar{\bar{\rho}}}. \tag{12}$$

The term ρ_s is the bidirectional reflectance factor (BRF), and $\bar{\rho}$, $\bar{\rho}'$ and $\bar{\bar{\rho}}$ are the surface hemispherical-directional, directional-hemispherical and hemispherical-hemispherical reflectance, respectively. These latter terms are also called coupling terms, as they are responsible for the coupling of atmospheric radiative transfer with the surface reflectance properties. They are calculated by angular integration of ρ_s weighted by the downwelling diffuse radiance. An analytical or numerical description of ρ_s is necessary for the calculation of $\bar{\rho}$, $\bar{\rho}'$ and $\bar{\bar{\rho}}$, while the rest of the parameters in equation (10) are already provided by ATLUT.

2.3 *Considerations on topographic effects*

The irradiance arriving at the surface is non-uniformly distributed over rough terrain, because of changes in surface slope and orientation. The separation between direct and diffuse fluxes and transmittance also enables the modelling of topographic effects in rough terrain. Equation (3) can be modified for rough terrain according to

$$E_g(x, y, z;\ \rho) = E_{dir}(z)\mu_{il}(x, y) + E^t_{dif}(x, y, z;\ \rho), \tag{13}$$

where z indicates the surface elevation, (x, y) the horizontal position, and $\mu_{il}(x, y)$ is the cosine of the illumination angle, defined as the angle between the solar rays and the surface normal vector ($\mu_{il}=\mu_s$ for a horizontal plane). $E^t_{dif}(x, y, z;\ \rho)$ is the diffuse irradiance arriving at a tilted plane at (x, y) with elevation z. The influence of the plane slope and orientation over the diffuse flux is corrected by adding a term which modulates the diffuse irradiance as a function of angles and atmospheric transmittance. Following Richter (1998), the Hay's model (Hay 1979) can be implemented to account for the anisotropic distribution of the diffuse irradiance. According to Hay's model, the diffuse irradiance on a tilted plane is given by

$$E^t_{dif}(x, y, z;\ \rho) = E_{dif}(z;\ \rho)\left[t^{\downarrow}_{dir}(z)\mu_{il}(x, y) + \left[1 - t^{\downarrow}_{dir}(z)\mu_s\right]\frac{1+\mu_n(x, y)}{2}\right], \tag{14}$$

where $E_{dif}(z)$ is the isotropic diffuse flux arriving at a flat surface at height z, $t^{\downarrow}_{dir}(z)$ is the transmittance for direct radiation from the Sun to the target, and $\mu_n(x, y)$ the cosine of the angle subtended between the surface normal vector and the vertical direction. The diffuse solar flux at the surface is compounded by a linear combination of two contributions, one coming from the circumsolar diffuse irradiance from the solid angle near the Sun, and the other is an isotropic contribution for the remaining sky dome (Richter 1998). It can be stated that $E^t_{dif}(x, y, z) \simeq E_{dif}(z)$ if the surface tilt angle is small, with the limit case $E^t_{dif}(x, y, z) = E_{dif}(z)$ for flat surfaces. The term $t^{\downarrow}_{dir}(z)$ can be calculated as the ratio between E_{dir} and the solar extraterrestrial irradiance, while a geolocated digital elevation model (DEM) must be used to derive μ_{il} and μ_n.

2.4 *Considerations on adjacency effects*

The adjacency effect is caused by photons reflected by the surroundings of the observed target which appear to be coming directly from the target itself because of atmospheric multiple scattering. A traditional statement of the problem can be found, for instance, in Dave (1980); Mekler and Kaufman (1982); Kaufman (1984). Adjacency effects lead to a loss of contrast in heterogeneous areas: dark surfaces look brighter because photons coming from the adjacent brighter surfaces enter into the sensor line of sight, while bright surfaces appear darker because the photons escaped from the observer's line of sight are not counterbalanced by those coming into it. The magnitude of this effect depends directly on the atmospheric turbidity and the surface heterogeneity.

A simple and efficient formulation of adjacency effects can be implemented if the transmittance for direct and diffuse radiation are decoupled (Richter 1990; Vermote *et al.* 1997a). It consists of modelling the at-sensor radiance as a linear combination of the photons coming directly from the target and those coming from areas adjacent to the target and scattered into the sensor direction. Following Vermote *et al.*

(1997a) notation, equation (4) can be rewritten as

$$L_{\mathrm{TOA}} = L_{\mathrm{p}}(0) + \frac{1}{\pi}\frac{\left[\rho t_{\mathrm{dir}}^{\uparrow} + \bar{\rho} t_{\mathrm{dif}}^{\uparrow}\right] E_{\mathrm{g}}(0)}{1 - S\bar{\rho}} \tag{15}$$

where ρ is the target reflectance and $\bar{\rho}$ the background reflectance. If ρ^u is the surface reflectance neglecting the adjacency effect (assumption of an infinite uniform target) which appears in equation (4), and we assume $S\bar{\rho} \ll 1$, the product $\rho^u T^{\uparrow}$ can be associated to the linear combination

$$\rho^u T^{\uparrow} = \rho t_{\mathrm{dir}}^{\uparrow} + \bar{\rho} t_{\mathrm{dif}}^{\uparrow} \tag{16}$$

by comparing equations (4) and (15). The surface reflectance free from the adjacency effect is then calculated as

$$\rho = \rho^u + \frac{t_{\mathrm{dif}}^{\uparrow}}{t_{\mathrm{dir}}^{\uparrow}}[\rho^u - \bar{\rho}], \tag{17}$$

The background contribution is formally given by

$$\bar{\rho} = \int_{-\infty}^{\infty}\int_{-\infty}^{\infty} f(r(x, y))\rho(x, y)\, dx\, dy \tag{18}$$

where $r(x, y)$ indicates the distance of a given background pixel at (x, y) to the observed pixel, located at (0, 0), and $f(r)$ is the atmospheric point spread function, which establishes the contribution of the environment to the registered TOA radiance. It depends on the atmospheric state and the observation configuration.

2.5 *Considerations on the design of a general purpose atmospheric LUT database*

The compilation of a general purpose atmospheric LUT database is very useful, especially for the operational atmospheric processing of large amounts of data. This is one of the main applications of the ATLUT code. One reason is that current-technology hyperspectral instruments frequently do not have stable spectral band positions due to temperature effects, thus requiring a corresponding update of the radiative transfer (RT) terms. This spectral resampling can be performed in a very short time if a properly designed high spectral resolution ('monochromatic') database is available. A second reason is that a high resolution database can be used for other hyperspectral sensors as well if the spectral coverage and resolution of the database are sufficient. The following list summarizes design criteria for general-purpose applications:

- a large spectral coverage, typically 400–1000 nm, or 400–2500 nm;
- a narrow spectral sampling grid to support a range of hyperspectral instruments, e.g., a 0.5 nm grid for instruments with spectral bandwidths of 3–5 nm (or higher);
- a wide range of solar geometries (zenith angle range 0–70°);
- a proper range of sensor view (tilt) geometries, and relative azimuth angles, if tilt sensors are to be supported;
- a range of ground elevations, e.g., sea level to 2.5 km above sea level;
- a range of aerosol optical thickness (AOT at 550 nm = 0.05–0.70), or equivalently, a range of visibilities (VIS = 10–200 km);

- a range of atmospheric columnar water vapour, e.g., 0.3–5 $g\,cm^{-2}$.

Depending on the intended range of applications, other requirements might comprise different aerosol types (e.g., rural, urban, maritime) and, for airborne systems, calculations for different flight altitudes. As a consequence, a general-purpose database has to stretch over a 6-to-8 dimensional parameter space with tens of thousands or several hundred thousand grid points. Therefore, the compilation of such a database is a large computing effort, but it pays off if it can be used for a number of instruments or even for one instrument where frequent spectral resampling is required.

3. Results

3.1 *Comparison of radiative transfer algorithms in MODTRAN4*

MODTRAN4 offers several algorithms to calculate the radiative transfer through the Earth's atmosphere. For multiple scattering calculations, Isaacs 2-stream (Isaacs *et al.* 1987), DISORT (Stamnes *et al.* 1988) with a variable number of streams, and scaled-DISORT are implemented in MODTRAN4. These are multiple scattering codes basically intended for spectral regions with minor absorption. Special attention is paid to the scaled-DISORT option. It performs a set of DISORT runs for some given wavelengths in order to correct the results obtained from the faster but less accurate Isaacs 2-stream algorithm (Isaacs *et al.* 1987). The scaled-DISORT approach relies on the smooth spectral dependence of multiple scattering. This leads to accurate calculations in those spectral regions where scattering dominates against absorption, although a loss in accuracy is found in those wavelengths where strong gaseous absorptions take place. In addition, the correlated-k (CK) method is available for increased accuracy in strong atmospheric absorption regions (Berk *et al.* 1998). It can be combined with the three multiple scattering algorithms, and spectral databases of different resolutions (1, 5, 15 cm^{-1}.) In principle, it is clear that the most accurate algorithm combination is DISORT/CK with the 1 cm^{-1} database. However, this leads to prohibitive calculation times if, for example, a large database of atmospheric LUTs has to be compiled.

This section presents selected results to demonstrate that the scaled DISORT with eight streams (S-8) achieves relative errors in the TOA radiance of 7% and 4% (with respect to the reference algorithm CK D-8, i.e., CK DISORT with eight streams) for the 5 nm and 10 nm bandwidths, respectively, while the CK S-8 achieves relative errors of less than 1% (10 nm bandwidth) and 2–4% (5 nm bandwidth). The execution time of the CK S-8 is reduced by a factor of 100 compared to the most accurate CK D-8 algorithm. Execution time is also considerably reduced if the CK S-8 is only applied to spectral absorption regions, and the S-8 to window regions. This means, a speed-optimized calculation partitions the total spectral coverage (usually 400–1000 nm or 400–2500 nm, depending on instrument) into window and absorption regions and runs MODTRAN4 with the appropriate algorithm and spectral resolution matched to each spectral sub-interval, see table 1. The $\Delta\lambda$, $\Delta\nu$, and 'database' of this table refer to the average wavelength sampling distance, constant wavenumber sampling, and MODTRAN4 band model/correlated-k database. In the spectral regions 1350–1450 nm and 1780–1950 nm a large sampling distance and the S-8 algorithm were chosen because these regions yield very low signals due to very strong water vapour absorption and are usually not used for a

Table 1. Accuracy/speed optimized spectral sub-regions for sensors with FWHM$\geqslant$5 nm. $\Delta\lambda$ is the average wavelength sampling distance, and $\Delta\nu$ the constant wavenumber sampling distance.

Spectral region (nm)	$\Delta\lambda$ (nm)	$\Delta\nu$ (cm^{-1})	Database (cm^{-1})	Algorithm
380–500	0.38	20	15	S-8
500–680	0.51	15	15	S-8
680–840	0.29	5	5	CK S-8
840–889	0.75	10	5	S-8
889–990	0.44	5	1	CK S-8
990–1080	0.53	5	1	S-8
1080–1240	0.67	5	1	CK S-8
1240–1351	0.50	3	1	S-8
1351–1449	0.98	5	5	S-8
1449–1779	0.52	2	1	S-8
1780–1949	1.74	5	5	S-8
1949–2099	0.41	1	1	CK S-8
2100–2302	0.48	1	1	S-8
2302–2500	0.58	1	1	CK S-8

quantitative evaluation. A broader wavenumber spacing is employed in spectral window regions. The sensor bandwith is represented by the Full Width at Half Maximum (FWHM) of the spectral response functions.

Figure 1 illustrates the atmospheric transmittance in the spectral region 400–2500 nm resampled to 10 nm. The absorption regions where table 1 uses the CK algorithm can be seen in this figure.

Figures 2–5 present selected results of different MODTRAN4 RT algorithms in different spectral regions evaluated for a TOA radiance with a surface reflectance of $\rho=0.15$. The simulation parameters are a mid-latitude summer atmosphere, water vapour column 2.9 $g\,cm^{-2}$, rural aerosol with AOT at 550 nm of 0.2, solar zenith angle (SZA) 40°, ground at sea level, sensor view zenith angle (VZA) 30° from a 650 km orbit, relative azimuth angles (RAAs) 0° (backscatter) and 90°, and bandwidths of 5 and 10 nm. Two spectral bandwidths were chosen to demonstrate the influence of the spectral bandwidth. Results are shown as deviations from the 'exact' reference case, i.e., CK D-8 with the highest spectral resolution BIN01 database and a 1 cm^{-1} sampling distance. With the exception of the 760 nm oxygen absorption region, the recommended CK S-8 algorithm with the BIN05 database has

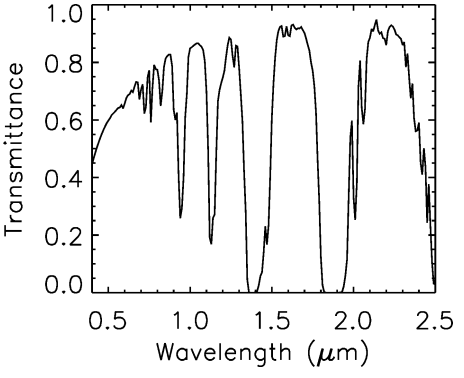

Figure 1. Spectral transmittance in the 400–2500 nm region resampled to 10 nm.

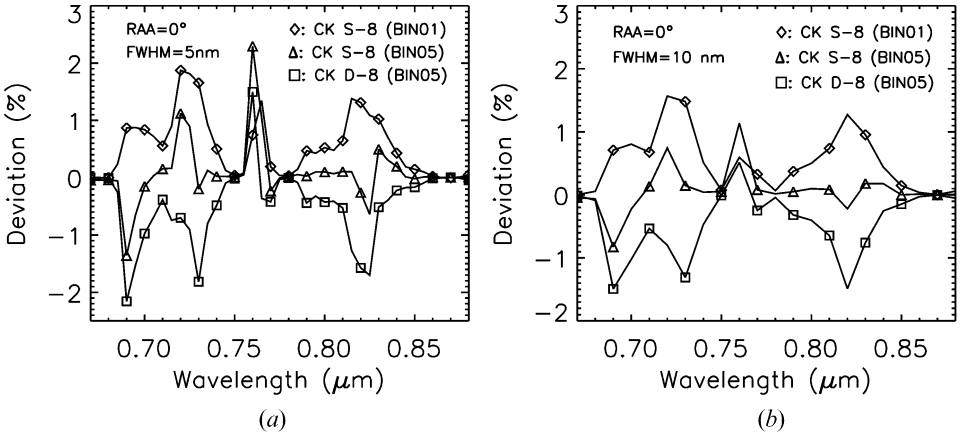

Figure 2. Deviation of TOA radiance $L_{TOA}(\rho=0.15)$ in the VNIR for different CK methods with respect to the reference (CK D-8 BIN01); *(a)* FWHM=5 nm, *(b)* FWHM=10 nm. RAA=0° is the relative azimuth angle for the backscatter geometry. Plot symbols distinguish the different cases, they do not indicate channel positions.

deviations less than 1.5% and 1% for the 5 nm and 10 nm bandwidths, respectively. In the oxygen region relative deviations reach about 2.4% for FWHM=5 nm, but are below 1% for the 10 nm bandwidth. Surprisingly, the CK S-8 BIN05 case has less deviations from the reference case than CK D-8 BIN05. This behaviour was also found for other aerosol loadings and solar geometries, it seems to be a systematic trend, probably caused by a partial error compensation of two approximations (S-8 versus D-8 and BIN05 versus BIN01).

Figure 3 shows results in the 880–1250 nm region. Here the BIN01 database is recommended for the CK S-8 case because it achieves more accuracy, but the 5 cm^{-1} sampling grid is employed. Of course, a 1 cm^{-1} sampling grid could also be used but with a time penalty of a factor 5 longer execution time. Deviations to the reference case reach levels of about 3%, both for the 5 and 10 nm cases. Deviations up to 4% are obtained for TOA radiances with $\rho=0.50$ instead of $\rho=0.15$ (figure not shown).

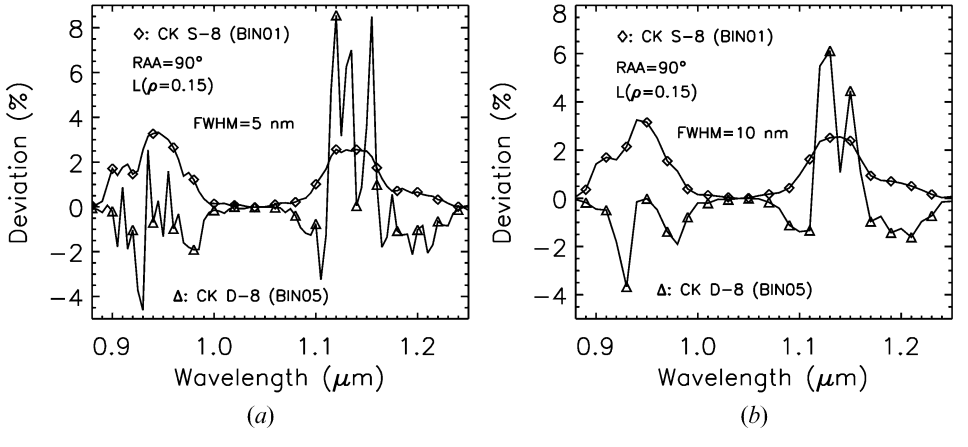

Figure 3. Deviation of TOA radiance $L_{TOA}(\rho=0.15)$ in the NIR for different CK methods with respect to the reference (CK D-8 BIN01); *(a)* FWHM=5 nm, *(b)* FWHM=10 nm.

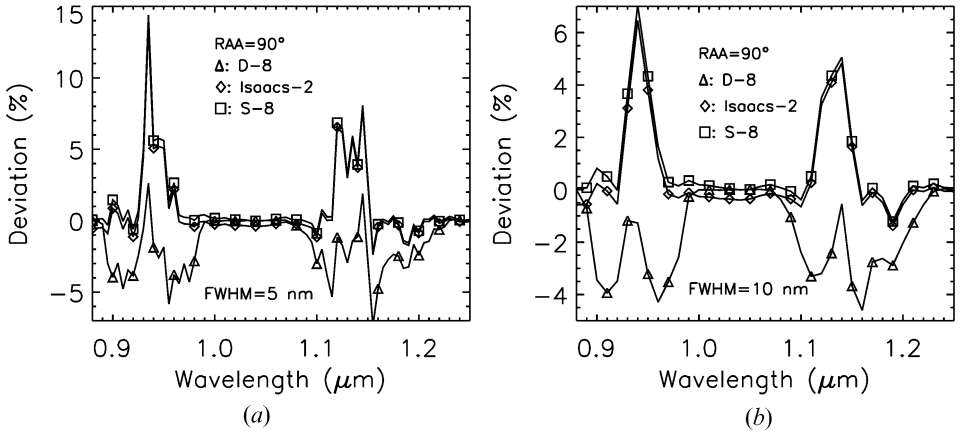

Figure 4. Deviation of TOA radiance $L_{TOA}(\rho=0.15)$ in the NIR for different non-CK methods with respect to the reference (CK D-8 BIN01); *(a)* FWHM=5 nm, *(b)* FWHM=10 nm.

The performance of the CK D-8 with the BIN05 database is worse than the CK S-8 BIN01 case.

Figure 4 presents results for the non-CK algorithms of S-8 and Isaacs 2-stream. Errors for the non-CK S-8 reach 14% and 7% for bandwidths of 5 nm and 10 nm, respectively. So they are substantially higher than for the corresponding CK cases.

Figure 5 shows results in the 1950–2500 nm region. Scattering effects are very small in this part of the spectrum, therefore all CK algorithms yield about the same results. So, only two cases are shown: the recommended CK S-8 and the non-CK Isaacs 2-stream, both with the BIN01 database and a 1 cm^{-1} sampling distance. The first algorithm achieves low deviations (<1%) with respect to the reference case, while the non-CK Isaacs yields deviations up to 8% and 6% for the 5 and 10 nm bandwidths, respectively.

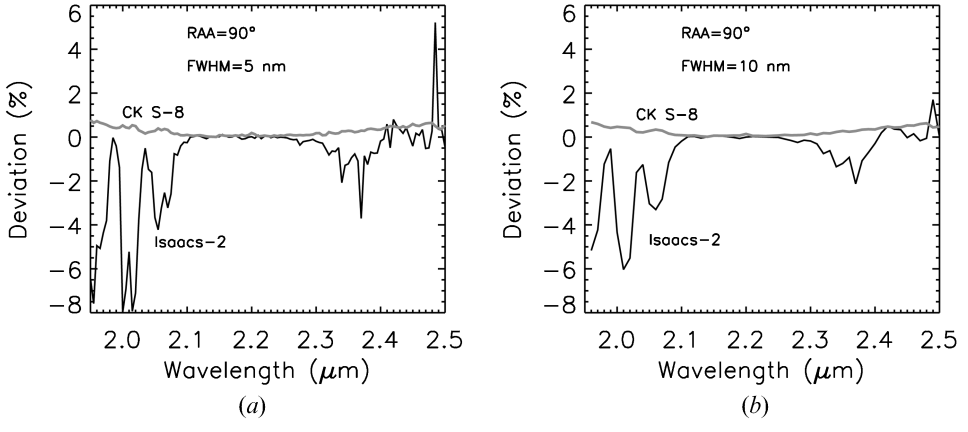

Figure 5. Deviation of TOA radiance $L_{TOA}(\rho=0.15)$ in the SWIR for CK S-8 and non-CK Isaacs with respect to the reference (CK D-8 BIN01); *(a)* FWHM=5 nm, *(b)* FWHM=10 nm.

3.2 *Application: derivation of LUTs for atmospheric correction of CHRIS/PROBA data*

The use of the methodology introduced in §2 is illustrated here by describing the derivation of LUTs for the atmospheric correction of CHRIS/PROBA data with the ATLUT code. CHRIS/PROBA data sets consist of five images acquired sequentially from five different view angles during a single overpass. The spectral configuration is set in advance through the selection of one of five possible acquisition modes, which define combinations of number, position and width of spectral channels, as well as spatial resolution and coverage. Moreover, for each of those acquisition modes the bands spectral position are expected to change due to thermal variations in the instrument from one acquisition to another. Therefore, large angular and spectral ranges must be covered by a LUT intended to be applied to the operational processing of CHRIS/PROBA data. In addition, frequent resampling of the 'monochromatic' LUT with the actual scene-dependent channel filter functions is required.

The LUT proposed in this work is built by sextuplets of $\left\{L_p, E_{\mathrm{dir}}, E_{\mathrm{dif}}, S, t_{\mathrm{dir}}^{\uparrow}, t_{\mathrm{dif}}^{\uparrow}\right\}$ for every breakpoint generated by the combination of the six input variables. Six free parameters from those discussed in §2.5 were selected as input for the defined LUT: VZA, SZA, RAA, surface elevation (ELEV), AOT at 550 nm (AOT@550) and columnar water vapour (CWV). It was considered that these parameters suffice to properly describe the scenario and the atmospheric state. The selected atmospheric model is the mid-latitude summer. Multiple scattering is computed making use of the DISORT scaling option with eight fluxes, as discussed in the previous section. Ozone and CO_2 are set to default values, $7.08\,\mathrm{g\,m^{-2}}$ and 380 parts per million by volume (ppmv), respectively. Ozone was discarded from the set of inputs as its low spatial and temporal variability do not lead to a significant impact on the signal, while adding an extra parameter to the LUT would have caused an increase in computation times. The rural aerosol model is also set in advance, as it provides the best representation of the atmospheric conditions expected in continental areas. Adding an extra variable accounting for the aerosol model, such as maritime or urban, is foreseen in order to cover those situations where a significant deviation from the rural model is expected. The calculations are performed using the default MODTRAN4 $5\,\mathrm{cm^{-1}}$ atmospheric data base. In order to decrease the LUT size, the output is degraded to 1 nm of spectral resolution and sampling. This is assumed to be sufficient for the subsequent resampling to CHRIS spectral response functions, which are typically around 10 nm. Sample E_{dir} and E_{dif} parameters provided by the LUT are displayed in figure 6. It can be stated that the atmospheric absorption features are well resolved despite the resampling to 1 nm.

The distribution of the breakpoints in the LUT is such that they cover the maximum variation rate in the parameters. Given a certain set of inputs, the values of the atmospheric parameters are calculated through linear interpolation in the six directions of the parameter space. It must be remarked that possible errors due to deviations from linearity at any combination of optical parameters and input values tend to compensate along the whole atmospheric correction process. For example, if a small bias in path radiance is introduced by linear interpolation during the estimation of AOT for the latter atmospheric correction, it is cancelled off to a large extent when the resulting AOT value is re-inserted in the process to calculate surface reflectance, as the same LUT and interpolation technique are used in forward and reverse modes.

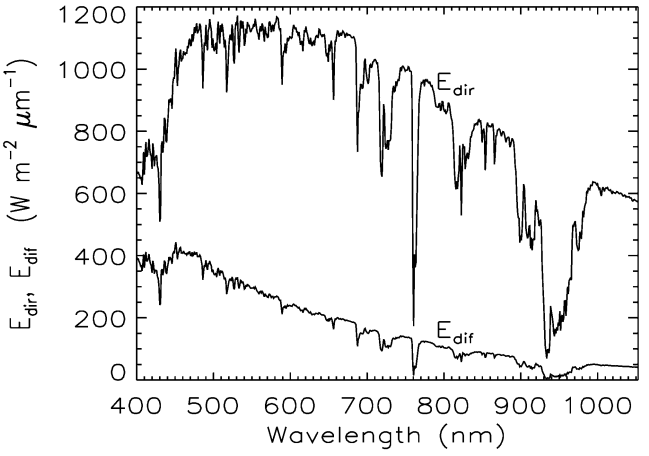

Figure 6. Direct and diffuse irradiance at the ground level provided by the LUT for the input values VZA=0°, SZA=30°, RAA=0°, ELEV=0.3 km, AOT@550=0.2 and CWV=2 g cm^{-2}.

The technique applied for the 6-D linear interpolation is a generalization of interpolation on a 2-D space to the case of a 6-D one. Each of the tabulated data points is weighted by the hyper-area spanned by the point of interpolation and the diametrically opposite grid point. The use of this formula is very convenient in computational terms, as it is easily implementable and does not involve a high computational burden. A recursive algorithm performing 1-D linear interpolation for each of the six dimensions was also tried, but it was discarded because it was neither as robust nor as efficient as the one with the weighting areas. The procedure starts looking for which of the hyper-cells contains the interpolation point. The data points to be used in the 6-D linear interpolation are the $2^6=64$ vertices of the hyper-cell. As different physical magnitudes are contained in the LUT, the dynamic ranges of each of the dimensions are normalized to [0, 1]. A matrix compounded by the six optical parameters in the 1 nm spectral grid is returned as interpolation result.

The optimum breakpoint positions for the six input parameters are presented in table 2. The number of breakpoints describing each dimension in the LUT is selected as a trade-off between sufficient sampling and LUT size. For this purpose, forward runs of ATLUT have provided the dependencies of physical magnitudes on the six free parameters. It was found that a number from four to eight breakpoints provides a sufficient sampling of the parameter space without leading to unaffordable computation times or LUT size.

For the selection of the breakpoint positions, their influence on scattering and absorption processes has been analysed. The atmospheric path radiance at the blue region (410 nm) is selected to describe scattering, while the ratio between pairs of absorption/reference bands describes absorption. Depending on the variable under study, scattering or absorption processes are considered. In particular, the path radiance is assumed to have the highest angular dependence, as it is mostly associated to first-order scattering. It is thus selected to analyse the best sampling for VZA, SZA and RAA. In addition, the path radiance is directly linked to the aerosol content, so it is also used to assess AOT. On the other hand, both scattering and absorption processes are considered for the analysis of the surface elevation, as it is strongly associated to Rayleigh scattering and to gaseous absorption. This one is

Table 2. Breakpoint positions in the LUT for the six input variables.

	No. 1	No. 2	No. 3	No. 4	No. 5	No. 6	No. 7	No. 8
VZA (°)	0	10	20	30	40	48	55	60
SZA (°)	0	10	20	35	50	60	70	–
RAA (°)	0	25	50	85	120	155	180	–
ELEV (km)	0	0.7	1.5	2.5	–	–	–	–
AOT@550	0.05	0.12	0.2	0.3	0.4	0.6	–	–
CWV ($g\,cm^{-2}$)	0.3	1	1.5	2	2.7	3.5	5	–

characterized by the depth of the O_2 absorption feature centred at 760 nm, calculated as the ratio between the direct irradiance inside and outside the absorption band (760 and 753 nm wavelengths, respectively). Finally, the columnar water vapour is represented by the differential absorption at 940 nm (reference at 890 nm). The results for the six input parameters are displayed in figure 7. It can be stated that linear interpolation can provide accurate results in most of the cases. The most critical one is the interpolation in RAA for low illumination angles, and the SZA for the backscatter geometry. The error compensation between forward and backward runs is expected to reduce the interpolation errors in those cases.

With this configuration, the resulting LUT consists of $8 \times 7 \times 7 \times 4 \times 6 \times 7 = 65\,856$ breakpoints, each of them containing six atmospheric optical parameters at 1 nm of spectral sampling. If this LUT is saved as 2-byte integer, the resulting size is about 510 Mbytes. This size may be too large if the LUT is to be delivered to external users as part of a processing software, so it was reduced by splitting the LUT into two: one of the sub-LUTs contained only L_p, which is the only variable depending on the RAA, while E_{dir}, E_{dif}, S, $t_{dir}^{\uparrow}$ and $t_{dif}^{\uparrow}$ are stored in a second LUT without the RAA-dimension. The total LUT size becomes then about 145 Mbytes.

4. Summary

A broad, comprehensive discussion about the use of MODTRAN4 for radiative transfer simulations in optical remote sensing has been presented in this work. Topics such as the calculation of the necessary atmospheric parameters for the inversion of TOA radiances, the formulation of directional, topographic and adjacency effects or the computational efficiency have been addressed.

One of the major problems of MODTRAN4 is that the atmospheric optical parameters in the standard output are coupled to the surface reflectance through multiple scattering effects. For this reason, they cannot be used in the inversion of TOA radiances. The transformation of the atmospheric parameters in the MODTRAN4 standard output into reflectance-independent quantities is achieved by some algebra performed over the outputs from two MODTRAN4 runs. This procedure is implemented as a code called ATLUT. Simple formulations of directional, topographic and adjacency effects have also been described. All of them make use of ATLUT outputs so that a consistent radiative transfer environment is built.

The compromise between accuracy and computation time is also a key point for MODTRAN4 users. The identification of the best MODTRAN4 execution configuration has been investigated. In particular, Isaacs, DISORT and scaled-DISORT multiple scattering algorithms, with and without correlated-k treatment of radiation absorption, have been compared to the reference case consisting of

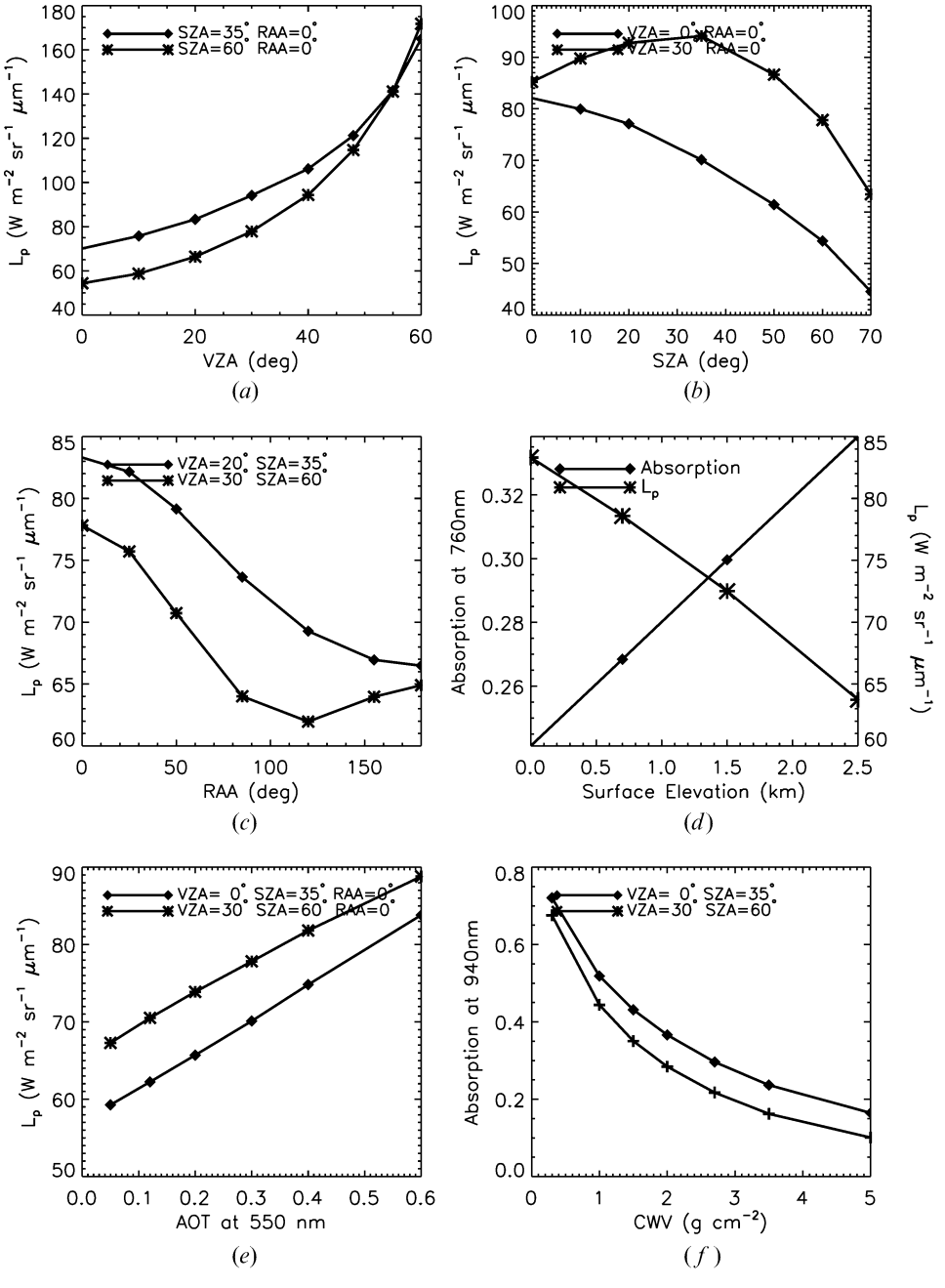

Figure 7. Sampling of scattering and absorption events by the six free parameters in the LUT. Scattering is characterized by the path radiance at 410 nm, and absorption is given by ratio between a band at the bottom of the absorption feature and one in the neighbouring continuum used as a reference.

DISORT with eight streams coupled to CK treatment and 1 cm^{-1} database. It has been demonstrated that the scaled DISORT with eight streams achieves relative errors in the TOA radiance of 7% and 4% for bandwidths of 5 nm and 10 nm, respectively, while the CK scaled-DISORT achieves relative errors of less than 1%

(10 nm bandwidth) and 2–4% (5 nm bandwidth), while the execution time of the CK scaled-DISORT is reduced by a factor of 100. Execution time is also considerably reduced if the CK scaled-DISORT is only applied to spectral absorption regions, and the non-CK scaled-DISORT to window regions.

The performance of the ATLUT code has been illustrated by the compilation of a LUT comprising atmospheric optical parameters and input variables for atmospheric correction. The design criteria for a general-purpose database for hyperspectral instruments are discussed including accuracy/speed and database size trade-off considerations. A case study was performed for the CHRIS/PROBA hyperspectral sensor to demonstrate the methodology for an example of practical interest.

Acknowledgments

This work has been partially developed in the framework of the project *Development of CHRIS/PROBA Modules for the BEAM Toolbox* (ESRIN Contract No. 20442/07/I-LG) and of the EnMAP hyperspectral mission preparatory activities (Kaufmann *et al.* 2008). The authors would also like to thank Prof. Mike Barnsley (1960–2007) for his important contribution to remote sensing, and to the CHRIS/PROBA mission in particular.

References

Adler-Golden, S.M., Matthew, M.W., Bernstein, L.S., Levine, R.Y., Berk, A., Richtsmeier, S.C., Acharya, P.K., Anderson, G.P., Felde, G., Gardner, J., Hoke, M.L., Jeong, L.S., Pukall, B., Mello, J., Ratkowski, A. and Burke, H.H., 1999, Atmospheric correction for short-wave spectral imagery based on MODTRAN4. *Proceedings of SPIE Conference on Imaging Spectrometry V*, **3753**, pp. 61–69.

Barnsley, M.J., Settle, J.J., Cutter, M., Lobb, D. and Teston, F., 2004, The PROBA/CHRIS mission: a low-cost smallsat for hyperspectral, multi-angle, observations of the Earth surface and atmosphere. *IEEE Transactions on Geoscience and Remote Sensing*, **42**, pp. 1512–1520.

Berk, A., Bernstein, L.S., Anderson, G.P., Acharya, P.K., Robertson, D.C., Chetwynd, J.H. and Adler-Golden, S.M., 1998, MODTRAN cloud and multiple scattering upgrades with application to AVIRIS. *Remote Sensing of Environment*, **65**, pp. 367–375.

Berk, A., Anderson, G.P., Acharya, P.K., Hoke, M.L., Chetwynd, J.H., Bernstein, L.S., Shettle, E.P., Matthew, M.W. and Adler-Golden, S.M., 2003, MODTRAN4 Version 3 Revision 1 User's Manual. Air Force Research Laboratory, Hanscom Air Force Base, MA, USA.

Börner, A., Wiest, L., Keller, P., Reulke, R., Richter, R., Schaepman, M. and Schläpfer, D., 2001, SENSOR: a tool for the simulation of hyperspectral remote sensing systems. *ISPRS Journal of Photogrammetry and Remote Sensing*, **55**, pp. 299–312.

Dave, J.V., 1980, Effect of atmospheric conditions on remote sensing of a surface nonhomogeneity. *Photogrammetric Engineering and Remote Sensing*, **46**, pp. 1173–1180.

Green, R., 1998, Spectral calibration requirement for Earth–looking imaging spectrometers in the solar-reflected spectrum. *Applied Optics*, **37**, pp. 683–690.

Green, R., Pavri, B. and Chrien, T., 2003, On-orbit radiometric and spectral calibration characteristics of EO-1 Hyperion derived with an underflight of AVIRIS and in situ measurements at Salar de Arizaro, Argentina. *IEEE Transactions on Geoscience and Remote Sensing*, **41**, pp. 1194–1203.

GUANTER, L., RICHTER, R. and MORENO, J., 2006, Spectral calibration of hyperspectral imagery using atmospheric absorption features. *Applied Optics*, **45**, pp. 2360–2370.

GUANTER, L., GONZÁLEZ, M.C. and MORENO, J., 2007, A method for the atmospheric correction of ENVISAT/MERIS data over land targets. *International Journal of Remote Sensing*, **28**, pp. 709–728.

HAY, J.E., 1979, Calculation of monthly mean solar radiation for horizontal and inclined surfaces. *Solar Energy*, **23**, pp. 301–307.

HENZING, J.S., KNAP, W.H., STAMMES, P., TEN BRINK H., KOS, G., SWART, D.P.J., APITULEY, A. and BERGWERFF, J.B., 2004, The effect of aerosols on the downward shortwave irradiances at the surface measurements versus calculations with MODTRAN4.1. *Journal of Geophysical Research*, doi:10.1029/2003JD004142.

ISAACS, R.G., WANG, W.C., WORSHAM, R.D. and GOLDENBERG, S., 1987, Multiple scattering LOWTRAN and FASCODE models. *Applied Optics*, **26**, pp. 1272–1281.

KAUFMAN, Y.J., 1984, Atmospheric effect on spatial resolution of surface imagery. *Applied Optics*, **23**, pp. 3400–3408.

KAUFMANN, H., SEGL, K., GUANTER, L., HOFER, S., FOERSTER, K.-P., STUFFLER, T., MUELLER, A., RICHTER, R., BACH, H., HOSTERT, P. and CHLEBEK, C., 2008, Environmental Mapping and Analysis Program (EnMAP) – Recent advances and status. *Proceedings of the IGARSS*, July, 2008, Boston, MA, USA.

KONDRATYEV, K.Y. and VAROTSOS, C., 1995, Atmospheric green house-effect in the context of global climate-change. *Nuovo Cimento della Società Italiana di Fisica C-Geophysics and Space Physics*, **18**, pp. 123–151.

MEKLER, Y. and KAUFMAN, Y.J., 1982, Contrast reduction by atmosphere and retrieval of nonuniform surface reflectance. *Applied Optics*, **21**, pp. 310–316.

MIESCH, C., POUTIER, L., ACHARD, V., BRIOTTET, X., LENOT, X. and BOUCHER, Y., 2005, Direct and inverse radiative transfer solutions for visible and near-infrared hyperspectral imagery. *IEEE Transactions on Geoscience and Remote Sensing*, **43**, pp. 1552–1562.

MILLER, C.J., 2002, Performance assessment of ACORN atmospheric correction algorithm. *Proceedings of SPIE Conference on Algorithms and Technologies Multispectral, Hyperspectral and Ultraspectral Imagery*, **4725**.

NICODEMUS, F.E., RICHMOND, J.C., HSIA, J.J., GINSBERG, I.W. and LIMPERIS, T., 1977, Geometrical considerations and nomenclature for reflectance. National Bureau of Standards, US Department of Commerce, Washington, DC, USA.

OGUNJOBI, K.O. and KIM, Y.J., 2007, Aerosol characteristics and surface radiative forcing components during a dust outbreak in Gwangju, Republic of Korea. *Environmental Monitoring and Assessment*, doi:10.1007/s10661-007-9733-z.

RICHTER, R., 1990, A fast atmospheric correction algorithm applied to Landsat TM images. *International Journal of Remote Sensing*, **11**, pp. 159–166.

RICHTER, R., 1998, Correction of satellite imagery over mountainous terrain. *Applied Optics*, **37**, pp. 4004–4015.

RICHTER, R. and SCHLAEPFER, D., 2002, Geo-atmospheric processing of airborne imaging spectrometry data. Part 2: atmospheric/topographic correction. *International Journal of Remote Sensing*, **23**, pp. 2631–2649.

STAENZ, K. and WILLIAMS, D.J., 1997, Retrieval of surface reflectance from hyperspectral data using a look-up table approach. *Canadian Journal of Remote Sensing*, **23**, pp. 354–368.

STAMNES, K., TSAY, S.C., WISCOMBE, W. and JAYAWEERA, K., 1988, A numerically stable algorithm for discrete ordinates method radiative transfer in multiple scattering and emitting layered media. *Applied Optics*, **27**, pp. 2502–2509.

VERHOEF, W. and BACH, H., 2003, Simulation of hyperspectral and directional radiance images using coupled biophysical and atmospheric radiative transfer models. *Remote Sensing of Environment*, **87**, pp. 23–41.

VERHOEF, W. and BACH, H., 2007, Coupled soil-leaf-canopy and atmosphere radiative transfer modeling to simulate hyperspectral multi-angular surface reflectance and TOA radiance data. *Remote Sensing of Environment*, **109**, pp. 166–182.

VERMOTE, E.F., EL-SALEOUS, N., JUSTICE, C.O., KAUFMAN, Y.J., PRIVETTE, J.L., REMER, L., ROGER, J.C. and TANRÉ, D., 1997a, Atmospheric correction of visible to middle infrared EOS-MODIS data over land surface: Background, operational algorithm and validation. *Journal of Geophysical Research*, **102**, pp. 17131–17141.

VERMOTE, E.F., TANRÉ, D., DEUZÉ, J.L., HERMAN, M. and MORCRETTE, J.J., 1997b, Second Simulation of the Satellite Signal in the Solar Spectrum, 6S: An overview. *IEEE Transactions on Geoscience and Remote Sensing*, **35**, pp. 675–686.